*Journal of Engineering Mathematics* **29**: 161–179, 1995.



# Interfacial waves and hydraulic falls: Some applications to atmospheric flows in the lee of mountains

SHAUN R. BELWARD* and LAWRENCE K. FORBES

*Centre for Industrial and Applied Mathematics and Parallel Computing, Department of Mathematics, The University of Queensland, Queensland, 4072, Australia*

Received 21 April 1993, Accepted in revised form 17 April 1994

**Abstract.** Two dimensional flow of a layer of constant density fluid over arbitrary topography, beneath a compressible, isothermal and stationary fluid is considered. Both downstream wave and critical flow solutions are obtained using a boundary integral formulation which is solved numerically by Newton's method. The resulting solutions are compared against waves produced behind similar obstacles in which the compressible upper layer is absent (single layer flow) and against the predictions of a linearised theory. The limiting waves predicted by the full non-linear equations are contrasted with those predicted by the forced Korteweg–de Vries theory. In particular, it is shown that at some parameter values a multiplicity of solutions exists in the full nonlinear theory.

## 1. Introduction

This work is related to the problem presented by Forbes and Belward [1] where waves at the interface between a heavy fluid of constant density and a lighter compressible fluid were investigated. The authors sought progressive periodic waves in this system of fluids in which the lower layer flowed beneath a stationary and isothermal upper layer. This model was intended to approximate the atmosphere under certain conditions, one of which could be the result of a distant thunderstorm expelling a downdraft of cool relatively dense air beneath a mass of warm less dense air. The mechanism of generation of these waves was not considered; one possibility is that these waves form in the lee (i.e. downstream) of a mountain or range of mountains.

Literature on the lee wave problem is now wide and varied. Many approximate theories have been suggested and many experimental and observational reports written. The early review article of Corby [2] details the experiences of pilots in gliders and powered aircraft, and summarises the theoretical work available up to that time. These theories involved linearising the equations for gas dynamics and approximated the downstream disturbances over small obstacles only. More recent contributions have focussed upon solving non-linear versions of the problem, in which large amplitude waves are permitted. Long [3] found that the governing equations could be reduced to a single linear equation if the upstream flow satisfied certain conditions. This enabled finite amplitude solutions to be obtained from a linear equation, and subsequent work using this approach may be found in Miles [4, 5] and Lilly and Klemp [6]. Vergeiner [7] linearised the equations for frictionless, adiabatic flow, but used a non-linear boundary conditions on the surface of the mountain. It was later shown by Smith [8] that these models can dramatically underestimate lee wave amplitude.

* Present address: Department of Mathematics and Statistics, James Cook University of North Queensland, Townsville, Queensland 4811, Australia.

The simplest model involving surface waves results from considering a single layer of constant density fluid flowing over the given topography. The literature in this area is extensive and the full non-linear problem has been solved for many topographical shapes by Forbes [9], Dias and Vanden-Broeck [10], and King and Bloor [11] who used a generalisation of the Schwarz–Christoffel transformation to solve the problem for arbitrary topography. Shen [12] considered two layers of fluid, each of constant density, flowing over topography and used a forced Korteweg–de Vries equation to solve for the shape of the upper free surface and the interfacial surface. The fully non-linear problem with two layers of constant density fluid flowing over arbitrary topography has been solved recently by Belward and Forbes [13], for a fixed upper surface and an interfacial surface of unknown location. This problem was solved using a boundary integral technique similar to that in the present paper. The two fluid layers in these last two papers could again arise as cool and relatively dense air associated with the downdraft from a thunderstorm is forced over a mountain.

Another phenomenon associated with airflow over mountains is that of the severe downslope windstorm. Again, many case studies have been made in this area, such as the recent article by Ikawa and Nagasawa [14]. Smith [15] used Long's equation as a mathematical model for this critical flow, and Peltier and Scinocca [16] linearised the equations for an inviscid, nonheat conducting, ideal gas, assuming small perturbations to the lee-averaged mean state of the storm, although non-linear boundary conditions were retained. Forbes [17, 18] calculated critical flow solutions for single and two layer flows, respectively, over a semi-circular obstruction. Here each layer consisted of a constant density fluid flowing irrotationally, and the full nonlinear problem was solved using a boundary integral formulation.

In the present paper we employ the structure of the atmosphere used by Forbes and Belward [1], to look at the generation of lee waves by topography, and the possible critical flow regimes. Our method enables calculation of flow conditions downstream of an arbitrarily shaped obstacle, and it is therefore not restricted by a formulation requiring a specific topography, as is the work of Forbes [9] and Dias and Vanden-Broeck [10]. In Section 2 the downstream wave problem is formulated as a system of two coupled integrodifferential equations which are required to be solved subject to certain conditions on the interface and far upstream. This permits a simpler treatment of general bottom topography than the conformal mapping approach adopted by King and Bloor [11]. The parameters governing the flow are required to satisfy certain physical conditions, which are mentioned in Section 3 as well as the constraints that the linear solution places on the parameters in order that lee waves are obtained. The numerical method is then presented, followed by an analysis of the behaviour of the nonlinear solutions. Comparison are made between the linear and nonlinear solutions and how each changes as the parameters are varied. An important check on our results is made by comparing the profile of the waves in the lee of a mountain obtained by our method, with the profile of the waves that were considered by Forbes and Belward [1] when the mechanism of generation of the waves was not of concern.

In Section 4 we look at the critical flow (hydraulic fall) problem. Here the fluid has characteristics of uniform flow far upstream (as in the lee wave problem) and uniform flow of higher velocity and lower depth far downstream. This is formulated in much the same way as the downstream wave problem, resulting in the same integrodifferential equations. However, the conditions which those equations are required to satisfy downstream are more precise than in the corresponding lee wave problem, since the flow is simply uniform far downstream of the obstacle. Again comparisons are made with known results, and the behaviour of the solutions as the parameters are varied is investigated.

In Section 5, the flow of a single layer of fluid over an obstacle is discussed, so that comparisons can be made between limiting flow regimes predicted by a forced Korteweg–de Vries (fK–dV) equation used by Shen [12], and the limiting flows computed from the full non-linear equations. It will be shown that while in the fK–dV theory the critical flow solution represents the limiting case of the downstream wave solution, the critical flow solutions of the full non-linear equations represent an entirely different branch of solutions.

Section 6 contains our summary and discussion and mentions area of further research associated with the results presented in this paper.

## 2. Formulation - downstream waves

We consider a system consisting of a layer of constant density fluid flowing irrotationally over arbitrary topography, beneath a stationary and isothermal compressible upper layer of fluid. The profile of the topography is given by $y = B(x)$ where $x$ and $y$ are the horizontal and vertical coordinates respectively. The upper fluid extends to infinite height, and consists of an ideal gas at uniform temperature $T_0$ with gas constant $R$. The flow in the lower layer is two dimensional, and becomes uniform far upstream. We let subscript 1 refer to variables in the upper layer and subscript 2 refer to variables in the lower layer. Densities and pressures in each layer are $\rho_j$ and $p_j$, $j = 1, 2$, respectively. The interface between the two fluids, which is unknown at the outset, is located at $y = S(x)$ and the fluid velocity vector in the lower layer is denoted by $\mathbf{q}_2$. Far upstream this velocity is $c_2\mathbf{i}$ and the lower layer has height $H_2$. We define $P_{atm}$ to be the pressure at $y = 0$ far upstream of the obstacle; this corresponds to the usual barometric pressure at ground level. Only waves that are stationary with respect to the mountain are considered, so partial derivatives with respect to time are identically zero. This fluid system is shown in Fig. 1, for an actual solution obtained with the method presented in Section 3.

The variables above are non-dimensionalised using $H_2$ as the length scale and $c_2$ as the velocity scale. The lower layer then has an upstream uniform speed of 1 and an upstream

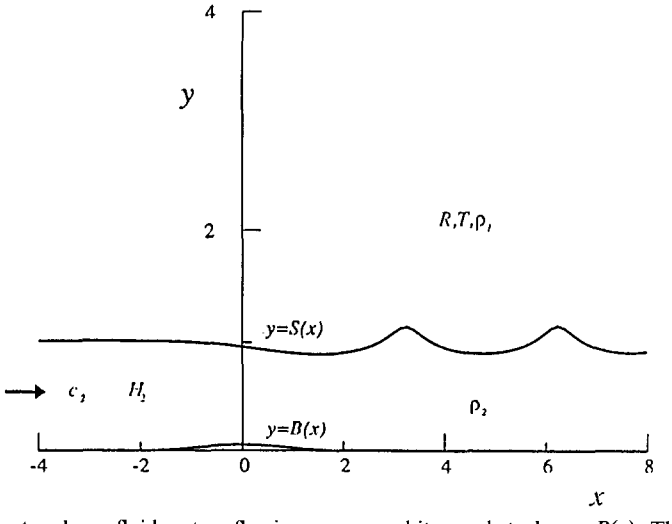


*Fig. 1.* A diagram of the two layer fluid system flowing over an arbitrary obstacle $y = B(x)$. The unknown interface $y = S(x)$ is to be obtained, and once known, enables any other quantity in either fluid layer to be calculated. This profile is a portion of an actual solution obtained with the parameter values, $h = 0.056$, $\alpha = 5$, $\beta = 1.1$ and $F = 0.5$. The scale on the vertical axis is twice that on the horixontal axis.

uniform height of 1 in this nondimensionalised coordinate system. We define three dimensionless parameters which describe properties of the flow,

$$F_2 = \frac{c_2}{\sqrt{gH_2}} \quad \text{the Froude number in the lower layer,}$$

$$\alpha = \frac{gH_2}{RT_0} \quad \text{the expansion parameter, and} \tag{2.1}$$

$$\beta = \frac{P_{\text{atm}}}{\rho_2 gH_2} \quad \text{the pressure ratio.}$$

Two additional parameters describe properties of the obstacle. These are denoted as $h$, the maximum height of the obstacle, and $L$ the obstacle half length. The following work proceeds with the same nondimensionalised variables introduced by Belward and Forbes [13].

Let $\phi_2$ be the velocity potential for the flow in the lower layer, which is assumed irrotational, so that the horizontal and vertical components of the velocity vector $\mathbf{q}_2$ are given by $u_2 = \partial\phi_2/\partial x$ and $v_2 = \partial\phi_2/\partial y$, respectively. Then within the lower layer, the continuity equation yields

$$\nabla^2\phi_2 = 0\,. \tag{2.2}$$

At the interface $y = S(x)$, there is no fluid exchange and so

$$\nabla\phi_2 \cdot \mathbf{n} = 0 \quad \text{on} \quad y = S(x)\,, \tag{2.3}$$

and on the bottom we have the condition of no penetration

$$\nabla\phi_2 \cdot \mathbf{n} = 0 \quad \text{on} \quad y = B(x)\,. \tag{2.4}$$

Here $\mathbf{n}$ refers to the normal vector to the free surface and bottom, respectively. Using the equation of state for an ideal gas, it may be shown that the pressure (which varies hydrostatically) in the upper layer is of the form

$$p_1 = A\exp[-\alpha y]\,. \tag{2.5}$$

Continuity of pressure at the fluid interface far upstream determines the constant $A$ to be

$$A = (\beta - 1)\exp\alpha\,,$$

and then the Bernoulli equation in the lower layer of fluid gives the interface condition

$$\frac{1}{2}F_2^2 q_2^2 + (\beta - 1)\exp[\alpha(1 - S(x))] + S(x) = \frac{1}{2}F_2^2 + \beta \quad \text{on} \quad y = S(x)\,. \tag{2.6}$$

The upstream conditions are

$$\mathbf{q}_2 \to \mathbf{i},\ S(x) \to 1 \quad \text{as} \quad x \to -\infty\,. \tag{2.7}$$

The full non-linear problem is thus defined by equations (2.2)–(2.7).

We introduce the complex variable $z = x + iy$, and the complex velocity potential is then $w_2 = \phi_2 + i\psi_2$ where $\psi_2$ is the stream function in the lower layer. Since the fluid in layer 2 is

incompressible and irrotational, $\phi_2$ and $\psi_2$ satisfy the Cauchy-Riemann equations. This means that $w_2$ is an analytic function of $z$. The conjugate complex velocity in the lower layer is given by $dw_2/dz = u_2 - iv_2$.

To calculate the location of the unknown interface, integrodifferential equations will be derived for the complex velocity on the boundaries and the interface of the fluid system. In formulating these equations an arclength, $s$, is used to parametrise the interface. Then along the interface

$$\left(\frac{dx}{ds}\right)^2 + \left(\frac{dy}{ds}\right)^2 = 1 . \tag{2.8}$$

The coordinates of the interface are $(x, S(x)) = (x(s), y(s))$ and the velocity components on the interface are given by

$$u_2 = \frac{dx}{ds}\frac{d\phi_2}{ds} \quad \text{and} \quad v_2 = \frac{dy}{ds}\frac{d\phi_2}{ds} .$$

Bernoulli's equation (2.6) on the interface becomes

$$\frac{1}{2}F_2^2\left(\frac{d\phi_2}{ds}\right)^2 + (\beta - 1)\exp[\alpha(1 - y(s))] + y(s) = \frac{1}{2}F_2^2 + \beta . \tag{2.9}$$

As in Belward and Forbes [13] the integrodifferential equations are obtained using Cauchy's integral formula. There are two such equations, each derived by integrating the function $\chi_2(z) = dw_2/dz - 1$ around a contour consisting of the interfacial surface, the bottom surface $y = B(x)$ and the vertical lines $x = \pm L$ with $L \to \infty$. The first of these equations has added to the contour a semicircle of vanishingly small radius centred on and excluding the point $z = z(s)$ on the interfacial surface and is given by

$$\oint_\Gamma \frac{\chi_2(z)\,dz}{z - z(s)} = 0 .$$

Taking the imaginary part gives

$$\begin{aligned}\pi[x'(s)\phi_2'(s) - 1] = &\int_{-\infty}^{\infty} \frac{[\phi_2'(\sigma) - x'(\sigma)](y(\sigma) - y(s)) + y'(\sigma)(x(\sigma) - x(s))}{(x(\sigma) - x(s))^2 + (y(\sigma) - y(s))^2}\,d\sigma \\ &- \int_{-\infty}^{\infty} \frac{B'(x)(x - x(s)) + (B(x) - y(s))(u_2(1 + B'(x)^2) - 1)}{(x - x(s))^2 + (B(x) - y(s))^2}\,dx .\end{aligned} \tag{2.10}$$

The second of the two equations has added to the contour a semicircle of vanishingly small radius excluding the point $z = z^* = x^* + iB(x^*)$ on the bottom surface and after taking the imaginary part is given by

$$\begin{aligned}\pi[u_2(x^*) - 1] = &\int_{-\infty}^{\infty} \frac{[\phi_2'(\sigma) - x'(\sigma)](y(\sigma) - B(x^*)) + y'(\sigma)(x(\sigma) - x^*)}{(x(\sigma) - x^*)^2 + (y(\sigma) - B(x^*))^2}\,d\sigma \\ &- \int_{-\infty}^{\infty} \frac{B'(x)(x - x^*) + (B(x) - B(x^*))(u_2(x)(1 + B'(x)^2) - 1)}{(x - x^*)^2 + (B(x) - B(x^*))^2}\,dx .\end{aligned} \tag{2.11}$$

Note in equation (2.10) the first integral has a Cauchy principal value singularity at $\sigma = s$

and in equation (2.11) the second integral has a Cauchy principal value singularity at $x = x^*$. Equations (2.10) and (2.11) are in fact linearly dependent, although both relationships are needed if arbitrary bottom profiles $y = B(x)$ are to be considered.

To find the location of the surface $y = S(x)$, we need to solve the two coupled integrodifferential equations (2.10) and (2.11) subject to the Bernoulli equation (2.9), the arclength condition (2.8) and the upstream asymptotic conditions (2.7). Once this surface is known, we may compute other quantities of interest, as will be shown in Section 3. For example a measure of the energy lost as the fluid flows over the obstacle is given by the nondimensionalised drag $G$, where

$$G = \int_{-L}^{L} p_2 B'(x)\, \mathrm{d}x\,.$$

Here we have assumed that the obstacle is in the interval $-L \leq x \leq L$ and $p_2$ is the pressure evaluated on the bottom $y = B(x)$. Using the Bernoulli equation on the bottom surface, this is written more conveniently as

$$G = \frac{-F_2^2}{2} \int_{-L}^{L} u_2^2 (1 + B'(x)^2) B'(x)\, \mathrm{d}x\,. \tag{2.12}$$

## 3. Numerical method and results

Before we solve the equations presented in Section 2, we describe some physical constraints on the parameter values. Looking at the definition of $\beta$ it is easy to see that $\beta \geq 1$, otherwise the atmospheric pressure at ground level would be less than the pressure due to the lower layer. The special case $\beta = 1$ corresponds to a single layer of constant density fluid flowing over the obstacle, so that the upper compressible fluid layer has zero weight. Using the equation of state for an ideal gas, equation (2.5) and the requirement that the density of the lower layer be greater than that of the upper layer to avoid the Kelvin–Helmholtz instability gives the condition

$$0 \leq \alpha(\beta - 1) \leq 1\,. \tag{3.1}$$

A linearised solution to equations (2.7)–(2.11) is easily derived for the case when the dimensionless mountain height $h$ is a small quantity. This linear solution is important in that it provides us with a valuable check on the results we obtain when the fully non-linear problem is solved numerically, and enables us to determine over which ranges the dimensionless parameters in the problem are likely to give downstream waves. The approach used to obtain the linear solution is similar to that presented in Belward and Forbes [13] and so will not be presented in detail here. The dispersion relation for the linear problem is given by

$$E(k_0) = 0 \tag{3.2}$$

where $k_0$ is the wavenumber of the downstream waves and

$$E(k) = F_2^2 k \cosh k - (1 - \alpha(\beta - 1)) \sinh k\,.$$

We note that this dispersion relation has the same form as when the upper layer is stationary,

with constant density and bounded above by a rigid lid. The dispersion relation (3.2) predicts solutions with downstream waves when

$$\frac{F_2^2}{1-\alpha(\beta-1)} < 1\,, \tag{3.3}$$

for disturbances of small amplitude.

The results presented in this paper will be for the mountain profile

$$B(x) = h\begin{cases} \frac{1}{2}\left(1+\cos\frac{\pi x}{L}\right) & -L \leqslant x \leqslant L \\ 0 \text{ otherwise}\,. \end{cases} \tag{3.4}$$

although the formulation in Section 2 permits an arbitrary topography. The linearised wave drag for this mountain profile is found using equation (2.12) and we obtain

$$G = \frac{h^2 F_2^2 \pi^4 k_0 \sin^2 k_0 L}{L^4\left(\frac{\pi^2}{L^2} - k_0^2\right)^2 (\sinh k_0 - k_0)\cosh k_0} \tag{3.5}$$

where the terms $O(h^3)$ have been ignored.

To obtain the nonlinear solution to equations (2.7)–(2.11) we use a numerical method similar to that of Forbes and Schwartz [19] and Belward and Forbes [13]. The interfacial boundary is sought at $N$ equally spaced points $s_1, s_2, \ldots, s_N$ with $s_1$ and $s_N$ approximating $-\infty$ and $\infty$, respectively. The method proceeds as follows.

We use Newton's method to solve for the unknowns $y'(s_2), \ldots, y'(s_N)$. A guess is made at $y'(s_j)$, $j = 2, \ldots, N$, while $y'(s_1) = 0$ is used to satisfy the condition of uniform flow far upstream. This initial guess may be that predicted by the linear solution, or $y'(s_j)$ values from a previous nonlinear solution, or even a vector of zeros.

The values $y(s_j)$ are found after numerical integration of the $y'(s_j)$ using the upstream condition $y(s_1) \approx y(-\infty) = 1$. The values $x'(s_j)$, $j = 2, \ldots, N$ are computed form the arc-length condition (2.8), and integrated to give $x(s_j)$ using the condition $x(s_1) = s_1$. Bernoulli's equation (2.9) then gives $\phi_2(s_j)$, $j = 2, \ldots, N$.

At this stage we need to define a grid on the bottom surface $y = B(x)$. This time the grid is more densely spaced over the obstacle, and so we take $M$ points, $x_1, x_2, \ldots, x_M$, not necessarily equally spaced, with $x_1$ and $x_M$ representing $-\infty$ and $\infty$, respectively. The integrodifferential equation (2.11) is discretised and solved for the unknown $u_2(x_j)$, $j = 2, \ldots, M$ at the $M-1$ points $x^* = x_{j+\frac{1}{2}} = \frac{1}{2}(x_j + x_{j+1})$, $j = 1, \ldots, M-1$. Note that we take $u_2(x_1) = 1$ to satisfy uniform flow conditions far upstream. Simpson's rule is used as the quadrature rule for evaluating the integrodifferential equation numerically after the singularity has been removed by subtraction.

The remaining integral equation (2.10) is used as a cost function, as all quantities are known at this stage. The initial guess $y'(s_j)$, $j = 2, \ldots, N$ is updated iteratively by Newton's method, until such time as the norm of the cost function falls below some predefined value.

Before we look at the numerical solutions generated by the above scheme, we consider a few of the properties of the linear solution, which predicts downstream waves with wavenumber $k_0$ when the inequalities (3.1) and (3.3) are satisfied. These solutions will be the same for any given mountain at any given Froude number $F_2$ if the expansion parameter

$\alpha$ and the pressure ratio $\beta$ are varied in such a way that $\alpha(\beta - 1)$ is constant. In addition the dispersion relation (3.2) shows that the linear solution will have waves of constant wavelength if the parameters are varied so that $F_2^2/(1 - \alpha(\beta - 1))$ is constant. Moreover, these waves will only vary in amplitude proportionally to $F_2^2$. These properties of the linear solution are also evident in the expression for the linear drag produced by the obstacle, although equation (3.5) shows that the linear drag varies as $h^2$, whereas the downstream wave amplitude is proportional to $h$.

The above numerical method was implemented on a computer and used to study the properties of the non-linear solution over a wide range of parameter values. We note that atmospheric flows occur in only a small region of the parameter space as follows: $\alpha$ is restricted so that $0.3 < \alpha < 0.6$, $\beta$ is restricted so that $2 < \beta < 3$ and the Froude number satisfies $F_2 < 0.25$ (assuming a lower layer with a height of 2 to 4 kilometres).

For small obstacles ($h = 0.001$) the solution was found to converge in only two iterations and to trace the linear solution almost exactly, which confirms the accuracy of our method for such disturbances. In most cases where the inequalities (3.1) and (3.3) were satisfied the solution was found to converge in five or fewer iterations. The only instances where convergence was slow occurred when a maximum or near maximum mountain height solution was being calculated. The maximum mountain height is that value of $h$ beyond which the numerical scheme fails to yield a solution, for a given set of physical parameters. The physical mechanism which results in the failure to obtain solutions for greater obstacle heights is clearly related to the mechanism restricting the amplitude of the atmospheric interfacial waves that were discussed in Forbes and Belward [1]. It is the formation of a stagnation point at the crest of the wave that ultimately causes the numerical method to fail. For obstacle heights greater than the maximum obstacle height it is expected that the waves will break so that no steady solution exists at these values of $h$.

Figure 2 highlights the effects of nonlinearity on the flow by comparing the linear and nonlinear solutions for a maximum mountain height solution, which is obtained with a

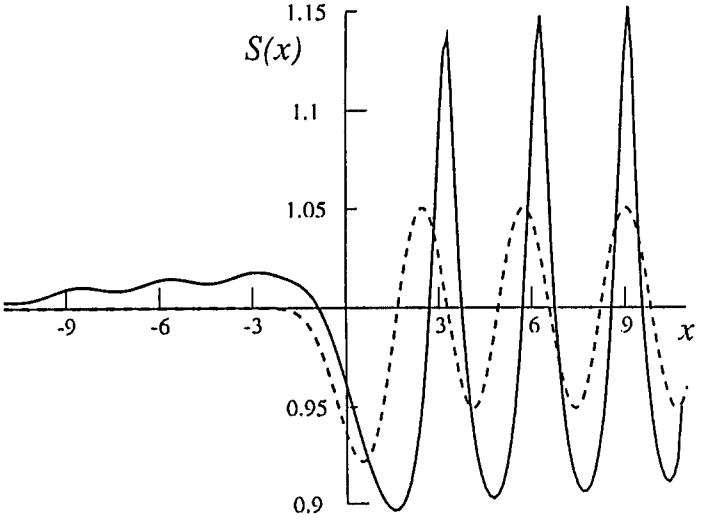


*Fig. 2.* A comparison of wave profiles for the parameters as in Fig. 1. The nonlinear profile (solid line) differs greatly from the linear profile (dashed line) for this relatively large mountain.

mountain height of $h = 0.056$, with the parameters values $\alpha = 5$, $\beta = 1.1$ and $F_2 = 0.5$. As for all results presented in this section the mountain has a half length $L = 2$. The non-linear features include very sharp crests, broad troughs and compression of the wavelength, and these are evident in all regions of the parameter space, including that encompassing atmospheric flows. Such characteristics are common to nonlinear free surface waves as can be seen in King and Bloor [11] and Forbes and Schwartz [19].

The behaviour of the nonlinear solutions was investigated by varying the parameters $\alpha$ and $\beta$ so that $\alpha(\beta - 1)$ was kept constant while the Froude number $F_2$ was kept constant. As predicted by the linear solution, the wave profiles were very similar for small mountains. However, as the mountain height increased the wave profiles changed as $\alpha$ and $\beta$ were changed at any given mountain height even if $\alpha(\beta - 1)$ was kept constant. Perhaps the main feature to note is that the maximum obstacle height for which solutions could be obtained decreased monotonically as $\alpha$ was increased, even if the wave profiles had similar wavelengths and amplitudes at any given mountain height. This can be seen in Table 1 where the maximum mountain height has been tabulated against $\alpha$ and $\beta$ when $\alpha(\beta - 1) = 0.5$.

A common feature of all the computational experiments performed was that for fixed $\alpha$ and $\beta$ the maximum mountain height for which a downstream wave solution could be obtained, in general, decreased as the Froude number increased. This decrease in maximum mountain height with increase in Froude number continued until the Froude number was near its limiting point for the linear theory where inequality (3.3) holds as an equality.

It is important to emphasise the qualitative differences between the waves generated on the surface of a single layer of constant density fluid, that is when $\beta = 1$, and those waves generated beneath a compressible atmosphere, when $\beta > 1$. Forbes and Belward [1] considered waves on the interface between a layer of constant density fluid and a layer of lighter compressible and stationary fluid. These waves were studied without regard for their mechanism of generation, enabling the authors to look at a single wavelength at a time. The solutions revealed that the waves beneath a compressible atmosphere had much broader troughs and sharper crests than the corresponding Stokes wave solution.

Figure 3 shows the comparison between the surface formed on a single layer of constant density fluid (the dotted graph) and an interfacial surface beneath a compressible atmosphere (the solid graph). The single layer solution was obtained with $F_2 = 0.70711 \approx 1/\sqrt{2}$ and $\beta = 1$ (note that $\alpha$ is irrelevant in this case as can be seen in equation (2.9)) while the solution beneath the compressible atmosphere was calculated with $F_2 = 0.5$, $\alpha = 5$ and $\beta = 1.1$. Both these sets of parameters were used on a mountain of height $h = 0.056$.

Figure 3 shows that, although the linear dispersion relation (3.2) predicts these waves will have the same wavelengths (since $F_2^2/(1 - \alpha(\beta - 1))$ is constant), the wavelength of the waves beneath the compressible atmosphere is slightly less than that of the waves on the single layer. Figure 4 shows the second wavelength of the downstream waves in each solution

*Table 1.* A comparison of maximum mountain heights for various expansion parameters $\alpha$ and pressure ratios $\beta$ when $\alpha(\beta - 1) = 0.5$ and $F_2 = 0.5$. The nonlinear drag $G$ is also shown

| $\alpha$ | $\beta$ | Max $h$ | Drag $G$ |
|---|---|---|---|
| 1 | 1.5 | 0.066 | $1.86 \times 10^{-3}$ |
| 2 | 1.25 | 0.061 | $1.55 \times 10^{-3}$ |
| 5 | 1.1 | 0.056 | $1.35 \times 10^{-3}$ |
| 10 | 1.05 | 0.041 | $6.30 \times 10^{-4}$ |

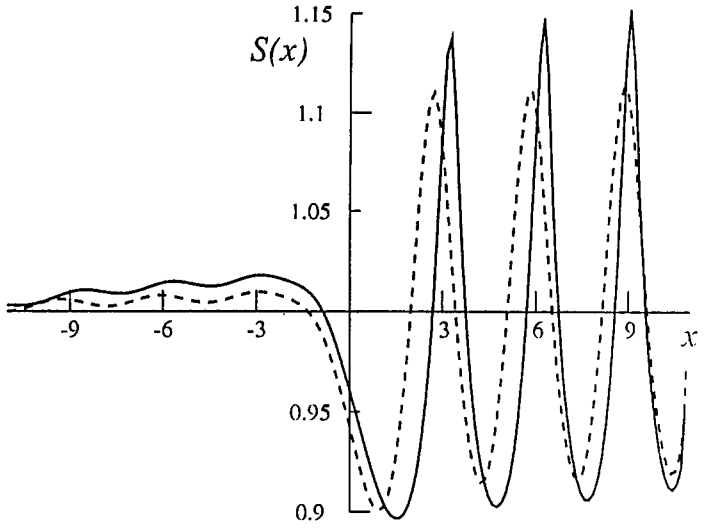


*Fig. 3.* A comparison of interface profiles for the cases when a compressible upper layer is present and when the upper layer is absent. The case when the compresible atmosphere is present has been calculated with the same parameter values as in Fig. 1 (solid line) and the single layer case has the parameter values $F_2 = 0.70711 \approx 1/\sqrt{2}$ and $\beta = 1$ (dotted line).

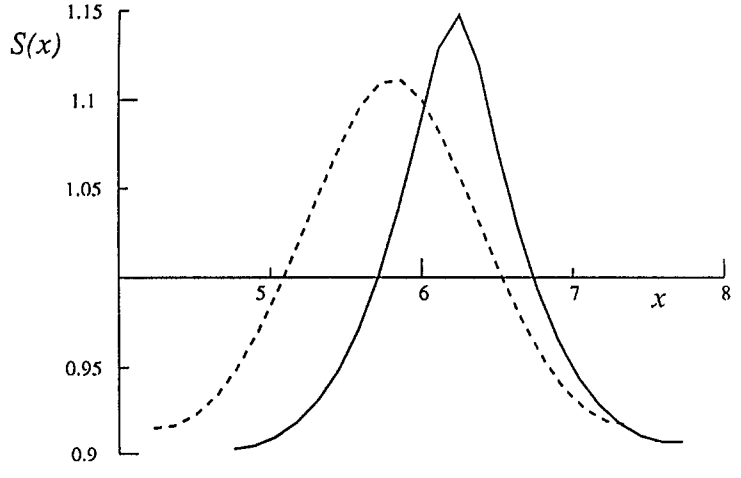


*Fig. 4.* A comparison of a single wavelength of the waves shown in Fig. 3. Note that the wave beneath the compressible fluid (solid line) has a sharper crest and broader trough than the single layer wave (dotted line).

in Fig. 3. Clearly the single layer solution has a more rounded crest, while the wave beneath the compressible atmosphere has a sharper crest and broader trough. These are exactly the characteristics observed by Forbes and Belward [1].

It should also be noted that the height at which the maximum obstacle solution was obtained was much larger for the single layer flow than that for the case when a compressible atmosphere overlay the lower fluid. Again this characteristics was observed by Forbes and Belward [1] where it was found that the limiting Stokes wave had a much higher amplitude than the corresponding limiting interfacial wave.

In Figs. 2 and 3 we note the occurrence of waves upstream of the obstacle, which can be directly attributed to numerical error. This phenomenon is well documented, for example

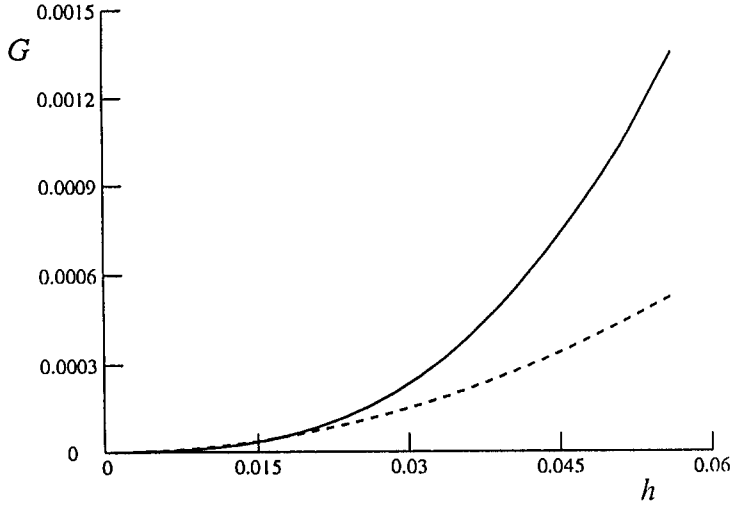


*Fig. 5.* A comparison of the nonlinear drag (solid line) and linear drag (dotted line) produced as the mountain height is increased. The parameter values are $\alpha = 5$, $\beta = 1.1$ and $F_2 = 0.5$.

see Forbes and Schwartz [19], and is known to be caused by the truncation of the interval over which the interface is sought. These waves can be removed by choosing appropriate values of $y(s_1)$ and $y'(s_1)$. In Fig. 2 we have varied $y(s_1)$ to minimise the upstream waves; however as this is a costly exercise computationally we have not pursued further the elimination of the upstream waves by varying $y'(s_1)$. The truncation of the interval over which the solution is found is also responsible for the lack of consistency shown in the last half wavelength of the downstream waves. Again this behaviour can be minimised by the correct choice of flow conditions at the truncation points.

Figure 5 shows a comparison of the linear and nonlinear drag produced by the obstacle for the parameter values $F_2 = 0.5$, $\alpha = 5$ and $\beta = 1.1$. This graph clearly demonstrates how non-linear effects increase the drag significantly for mountains of height greater than about $h = 0.02$, until the maximum mountain height is attained, at which the non-linear drag is nearly three times the linear drag. It is also of note that the drag produced by the mountain underneath a compressible atmosphere is less than that produced by the same obstacle during single layer flow.

## 4. Critical flow - formulation, numerical method and results

In this section we formulate the equations for the critical flow model, look at their numerical solution and the results obtained from computational experiments. Instead of seeking lee waves, the problem now is to find solutions where the flow becomes uniform very far downstream. The same atmospheric structure as in Section 2 is used with the same upstream flow conditions. We return momentarily to dimensional variables. Far downstream of the mountain we expect the interface to fall to a height of $y = \gamma H_2$ where $\gamma < 1$, and the fluid velocity to be given by $\mathbf{q}_2 = Vc_2\mathbf{i}$. Again the interface shape $y = S(x)$ is unknown at the outset. The fluid system is shown in Fig. 6, for an actual solution obtained using the numerical technique presented below.

Continuity requires that the volumes of fluid entering and leaving the system are equal, so that $c_2 H_2 = Vc_2 \gamma H_2$, from which it follows that

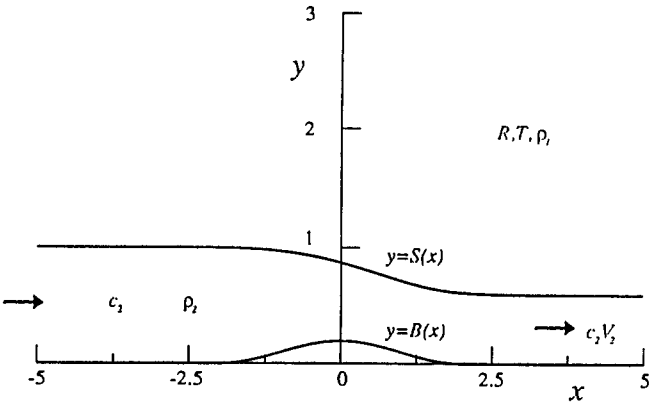


*Fig. 6.* A diagram of the critical flow problem. This profile is taken from an actual solution with the parameters given by $h = 0.2$, $\alpha = 2$ and $\beta = 1.25$. The scale on the vertical axis is twice that on the horizontal axis.

$$\gamma = \frac{1}{V}. \tag{4.1}$$

All the variables in this critical flow model are nondimensionalised in the same manner as in Section 2. The dimensionless parameters describing the flow are the five defined in Section 2, with the addition of the new parameter $V$ which is the non-dimensionalised downstream fluid speed. We proceed now purely with dimensionless variables.

The flow is described by equations (2.2)–(2.7) with the addition of the following downstream conditions which arise using equation (4.1):

$$\mathbf{q}_2 \to V\mathbf{i},\ S(x) \to \frac{1}{V} \quad \text{as} \quad x \to \infty. \tag{4.2}$$

Substituting these downstream conditions into the Bernoulli equation (2.6) gives

$$F_2 = \sqrt{\frac{2}{V^2 - 1}\left\{\beta - \frac{1}{V} - (\beta - 1)\exp\left[\alpha\left(1 - \frac{1}{V}\right)\right]\right\}} \tag{4.3}$$

which means that the upstream Froude number is determined by the downstream flow conditions.

Given $\alpha$ and $\beta$, we wish to determine the interface $S(x)$ which in turn gives the downstream uniform fluid velocity $V$ and upstream Froude number $F_2$. The parametrisation of the interface is carried out exactly as in Section 2, resulting in the same integrodifferential equations. Thus the equations to be solved are (2.10) and (2.11) subject to the Bernoulli equation (2.9), the arclength condition (2.8), and the upstream and downstream asymptotic conditions (2.7) and (4.2), while the Froude number is given by equation (4.3).

The numerical solution of these equations proceeds much in the same way as in Section 3. Since the mean level of the surface decreases in the lee of the obstacle, we need to estimate the downstream portions of the integrals in equations (2.10) and (2.11) to avoid loss of accuracy. This is done with the downstream asymptotic conditions (4.2). Since the interface shape lacks the complication of downstream waves, when critical flow is occurring, it is sufficient to use the trapezoidal rule for integration rather than Simpson's rule as in Section

3. This means that the singularities in equations (2.10) and (2.11) can simply be ignored as recognized by Monacella [20]. The drag for the critical flow case is easily calculated using equation (2.12).

Figure 7 shows the variation of froude number with obstacle height for the mountain given by equation (3.4) with half length $L = 2$. The expansion parameter has the value $\alpha = 2$, and the pressure ratio is $\beta = 1.25$. Clearly the Froude number decreases as the mountain height increases. The highest Froude number obtained with these parameter values was $F = 0.690$ with a mountain of height $h = 0.001$. The maximum possible Froude number is $F_2 = \sqrt{1 - \alpha(\beta - 1)} = 1/\sqrt{2}$, which is the value at which the flow becomes critical in the linearised theory. Hence, this Froude number corresponds to a mountain of zero height.

Figure 8 shows the increase of the drag with mountain height for the same parameter values as in Fig. 7. The drag increases almost linearly to a value of $G = 0.0287$ for a mountain of height $h = 0.45$. We note that the drag produced under critical flow is in general much larger than that when waves are formed downstream of the obstacle. However, direct comparison is hard as it is important to note that the Froude number changes as we move along the curve in Fig. 8, whereas in Fig. 5 the drag is being produced at constant Froude number.

In Fig. 9 some non-linear interfacial surface profiles are shown. Again the parameter values are as in the previous two figures. Clearly, the qualitative features of the solution remain the same as the mountain height is increased. The interface has negative slope over the region of the obstacle but is horizontal on either side. Downstream of the obstacle the fluid speed increases and the flow is supercritical. The slope of the interface over the mountain and the downstream fluid speed increase together as the mountain height is increased. These are all features noted by Forbes [17] when single layer flow over a semi-circular obstruction was considered.

The numerical technique has performed very well as can be seen from the quality of the interface profiles in Fig. 9. The only evidence of numerical error can be seen in the profiles for mountains of height greater than about $h = 0.4$ where the last few grid points are raised

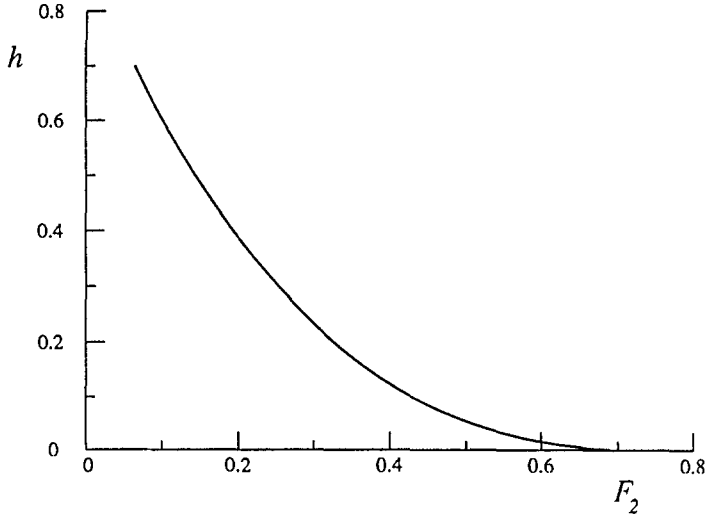


*Fig. 7.* A graph showing the dependence of Froude number on mountain height for the critical flow problem with $\alpha = 2$ and $\beta = 1.25$.

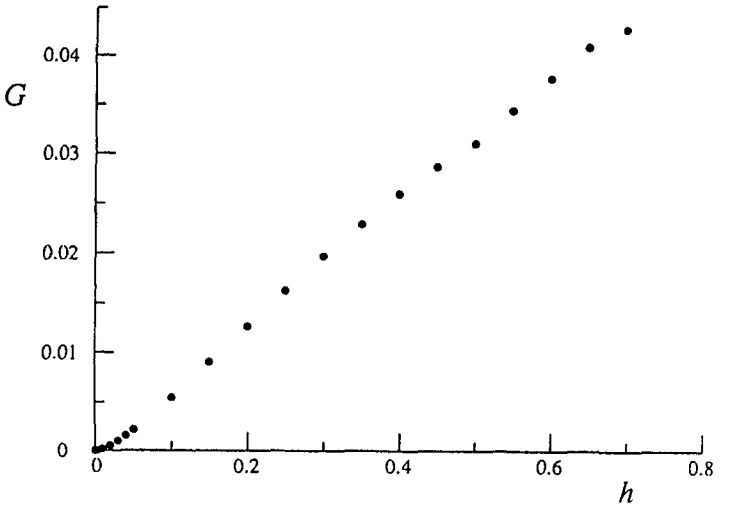


*Fig. 8.* A graph showing the variation of drag with mountain height for the parameter values as in Fig. 7.

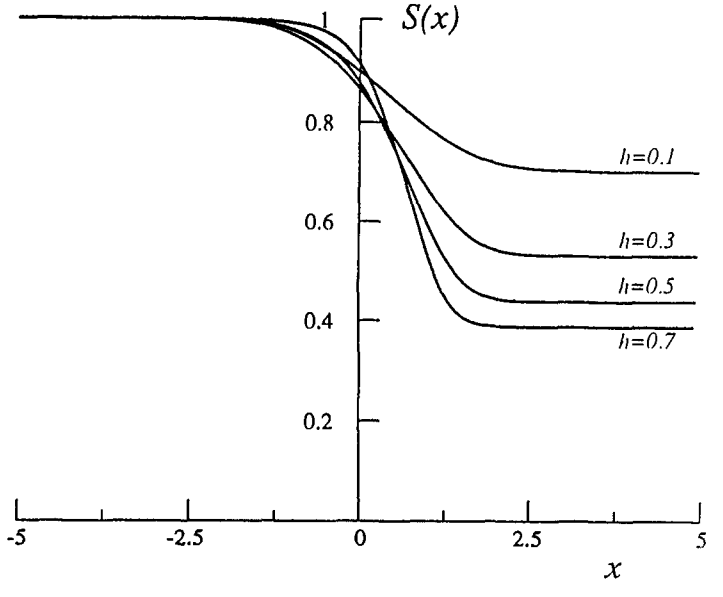


*Fig. 9.* Interface profiles for mountain heights $h = 0.1, 0.3, 0.5, 0.7$. The parameter values are as in Fig. 7.

higher than the points immediately to their left. This is due to the truncation of the integrals in equations (2.10) and (2.11), and was again noted by Forbes [17]. The failure of the numerical technique to compute solutions for mountains higher than $h = 0.7$ must be attributed to the difficulty of coping with high downstream fluid speeds and large interfacial slopes over the obstacle.

As in Section 3 we investigated the behaviour of the solutions when $\alpha$ and $\beta$ were varied so as to keep $\alpha(\beta - 1)$ constant. It was found that Froude number versus mountain height curves were very similar, especially for small obstacle heights. This highlights a certain predictive property of the linear dispersion relation, even for critical flows.

## 5. A comparison with Korteweg–de Vries theory

For the majority of this section we consider the special case when the upper layer has zero weight, that is, when $\beta = 1$. A comparison will be made between the predictions the full nonlinear equations make about the downstream flow and those obtained from a forced Korteweg–de Vries theory.

Shen [12] considered two layer fluid flow forced by an obstacle, or perhaps due to some over-pressure applied on the top surface. It was shown for small obstacles of low curvature that the full non-linear equations could be approximated by a forced Korteweg–de Vries equation. For subcritical flows (when $F_2 < 1$ for single layer flows) the fK–dV equation predicts downstream wave solutions for Froude numbers less than some Froude number $F_L$ called the cutoff Froude number. For any given obstacle this fK–dV theory predicts that, as the Froude number is increased, the wavelength of the downstream waves increases until $F_2 = F_L$, which point the wavelength has become infinite. This is the hydraulic fall solution that the fK–dV theory produces as a limiting case of the downstream wave solution. According to the fK–dV theory it is not possible to obtain a hydraulic fall solution at the same upstream Froude number at which a solution possessing downstream waves exists.

The obstacle we have considered in Sections 3 and 4 has in many cases been rather low and relatively small in curvature, and as such should be ideally suited to the fK–dV formulation. However Fig. 10 shows a result not predicted by this approximate theory. Two solutions are displayed in this figure, the first of which is a hydraulic fall solution occuring at a Froude number of approximately $F_2 = 0.8001$ for a mountain of height $h = 0.04$. The second solution is the downstream wave solution at exactly the same Froude number and same mountain height (note $\beta = 1$ as mentioned above, and $L = 2$). This clearly shows that in the full non-linear theory the hydraulic fall solution is not the limiting case of the

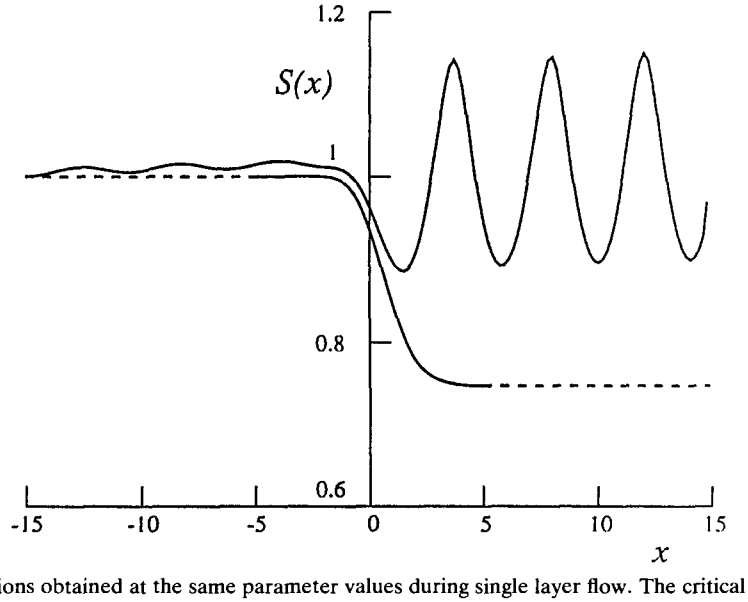


*Fig. 10.* Two solutions obtained at the same parameter values during single layer flow. The critical flow solution was obtained over the interval $-5 < x < 5$ and has been extended by hand (dotted lines). The parameter values are given by $h = 0.04$, $L = 2$ and $\beta = 1$. With these values the critical flow solution requires a Froude number of $F_2 \approx 0.8001$.

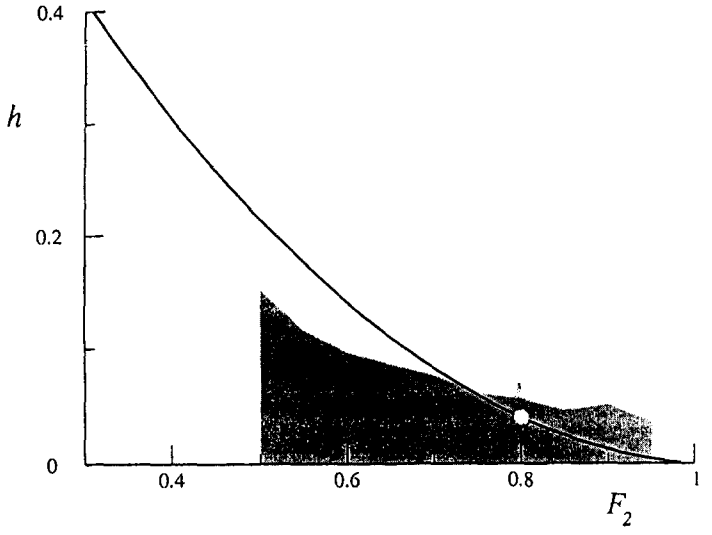


*Fig. 11(a).* A comparison of the Froude numbers at which critical flow solutions are obtained (solid line) with the Froude numbers at which downstream wave solutions can be obtained (shaded region) during single layer flow with $\beta = 1$ and $L = 2$. The position marked with an open circle represents the point at which the solutions in Fig. 10 were obtained.

downstream wave solutions; rather it represents an entirely different branch of solutions which may occur at the same parameter values as a downstream wave solution.

In Fig. 11(a), the existence of the two subcritical ($F_2 < 1$) solution types is represented in a parameter space consisting of the upstream Froude number $F_2$ and the mountain height $h$, for $\beta = 1$ and $L = 2$. Solutions possessing downstream waves have been computed within the shaded region on the figure, and the upper boundary of this shaded region corresponds to the maximum mountain height lee wave solution. We have investigated solutions in the interval of Froude numbers $0.5 < F_2 < 0.95$ in detail, but for reasons of numerical accuracy

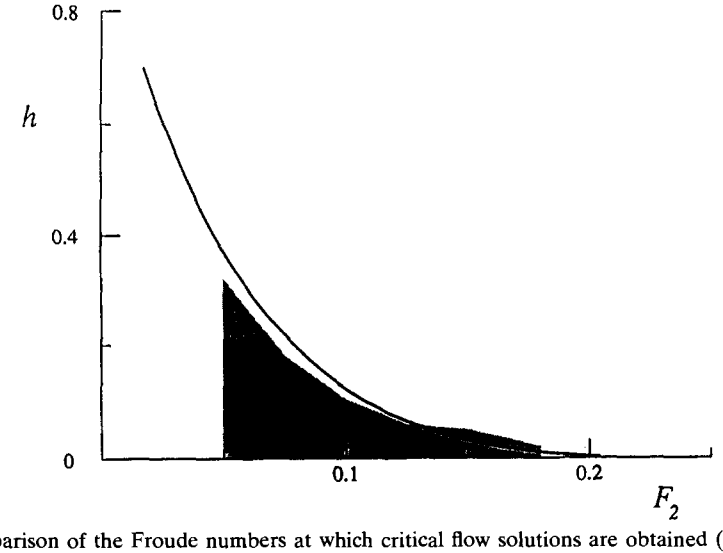


*Fig. 11(b).* A comparison of the Froude numbers at which critical flow solutions are obtained (solid line) with the Froude numbers at which downstream wave solutions can be obtained (shaded region) for a genuine atmospheric flow with $\alpha = 0.475$, $\beta = 3$ and $L = 2$.

and computational cost, a systematic study of solutions for other Froude numbers was not undertaken.

The line representing the branch of hydraulic fall solutions is also displayed in Fig. 11(a). Clearly it passes directly through the region in which downstream wave solutions occur, when $F_2$ is greater than about 0.72. The position marked as an open circle on the hydraulic fall curve is that at which the solutions in Fig. 10 are obtained. Again this highlights the fact that the critical flow solution is not a limiting case of the downstream wave solution and we have revealed a significant qualitative error in the fK–dV theory.

Figure 11(b) shows exactly the same behaviour of the two subcritical solution types when the parameters represent an atmospheric flow. In this figure, $\alpha = 0.475$, $\beta = 3$ and $L = 2$, and again the shaded region represents solutions possessing downstream waves while the solid line represents hydraulic fall solutions. The characteristic of multiple solutions is evident here when $F_2$ is greater than about 0.13 and clearly is not peculiar to single layer or non-atmospheric flows.

Clearly, the question is yet unresolved concerning which solution will actually occur if the parameters are such that both solutions are possible. This question is beyond the scope of the present paper. However, an experimental approach such as that employed by Forbes [17] may shed some light on the influence of conditions far upstream and downstream of the obstacle upon the solution type observed in practice.

## 6. Summary and discussion

In this paper we have developed a numerical method that calculates the flow of a constant density fluid over an arbitrary topography, beneath a compressible, isothermal and stationary fluid. This is intended to model atmospheric airflow over mountains and is an extension of the work of Forbes and Belward [1] where waves at the interface of two fluids with the same properties as those used here were considered without concern for their mechanism of generation.

The problem was formulated using a boundary integral technique where the unknown fluid velocity was calculated on the boundary of a truncated section of the lower layer after the equations had been discretised. Using this approach we were able to obtain solutions with lee waves and the corresponding hydraulic fall solutions. The downstream wave solutions showed non-linear characteristics not predicted by the linear theory. In particular the wave amplitude and wave drag in the non-linear theory were far in excess of the quantities predicted by the linear theory for all but the smallest mountains. The waves beneath the compressible atmosphere possessed sharp crests and long broad troughs, quite different from those in the linear theory, and notably different from the corresponding waves produced on a single layer of fluid flowing over the same topography. The computed wave profiles were compared to those obtained by Forbes and Belward [1] and were observed to possess the same characteristics as the waves found by these authors.

The critical flow solution was obtained by specifying the downstream flow conditions. This highly non-linear flow was calculated for obstacles of greater height than those for which the downstream wave solutions could be calculated, due to the fact that the downstream flow is uniform, unlike that when lee waves are produced. The drag produced during critical flow was found to be much greater than that produced when lee waves were generated.

An interesting feature of the critical flow and lee wave solutions was noted for the case

when the upper layer had zero weight. We were able to calculate both downstream wave solutions and hydraulic fall solutions for the same set of parameter values. This property is notably absent in the forced Korteweg–de Vries theory presented by Shen [12] where the critical flow solution is predicted to be a limiting case of the downstream wave solution. In the full non-linear theory it is expected that the limiting downstream wave solution represents the point at which wave breaking occurs, and we therefore expect no steady state solutions immediately above the shaded region in Fig. 11(a). The multiplicity of solutions was also noted for genuine atmospheric flows as shown in Fig. 11(b).

As mentioned in the previous section, the ability to produce two solutions at the same parameter values presents the interesting problem of predicting when each solution type may actually occur in practice. This is clearly open to further research. For definiteness, we have confined attention to the mountain profile (3.4), although our method is available for arbitrary obstacle shape, at no additional computational expense, and the influence of other topographies is currently under investigation. For example, it is almost certain that the region of overlap of critical flow and downstream wave solutions is smaller than that shown in Figs. 11(a) and (b) for some mountain profiles.

Another interesting problem arises when the upper compressible layer is no longer stationary. Boundary integrals would only be of use in the lower layer as the flow in the upper layer would not satisfy Laplace's equation. A model is currently being developed in which progressive periodic waves are formed on the interface between an upper compressible layer and a lower layer of constant density fluid, when the upper as well as the lower layer is free to move. The properties of lee waves in this expanded model have been studied without regard to the mechanism for their generation, and details will be published elsewhere.

The numerical method of this paper has been used to investigate flow over other mountain shapes. In particular flows over obstacles with profiles given by cubic splines were noted to exhibit the same behaviour as that observed in Section 5 for flow over cosine shaped obstacles. This implies that the multiple solutions discussed in Section 5 are not confined merely to trigonometric profiles but will be observed over a wide range of topographical features.

## Acknowledgement

This work was supported by an Australian Postgraduate Research Award.

## References

1. L.K. Forbes and S.R. Belward, Atmospheric interfacial waves. *Phys. Fluids Ser.* A 4 (1992) 2222–2229.
2. G.A. Corby, The airflow over mountains. A review of the state of current knowledge. *Quart. J.R. Met. Soc.* 80 (1954) 491–521.
3. R.R. Long, Some aspects of the flow of stratified fluids. *Tellus* 5 (1953) 42–58.
4. J.W. Miles, Lee waves in a stratified flow. Part 1. Thin barrier. *J. Fluid Mech.* 32 (1968) 549–567.
5. J.W. Miles, Waves and wave drag in stratified flows, *Proc 12th International Congress of Applied Mechanics.* Springer Verlag, Berlin (1969) 50–67.
6. D.K. Lilly, and J.B. Klemp, The effects of terrain shape on nonlinear hydrostatic mountain waves. *J. Fluid Mech.* 95 (1979) 241–261.

7. I. Vergeiner, An operational linear lee wave model for arbitrary basic flow and two-dimensional topography. *Quart. J. R. Met. Soc.* 97 (1971) 30–60.
8. R.B. Smith, The generation of lee waves by the Blue Ridge. *J. Atmos. Sci.* 33 (1976) 507–519.
9. L.K. Forbes, On the wave resistance of a submerged semi-elliptical body. *J. Eng. Math.* 15 (1981) 287–298.
10. F. Dias. and J.-M. Vanden-Broeck, Open channel flows with submerged obstructions. *J. Fluid Mech.* 206 (1989) 155–170.
11. A.C. King and M.I.G. Bloor Free streamline flow over curved topography. *Quart. J. Appl. Math.* 48 (1990) 281–293.
12. S.S.P. Shen, Forced solitary waves and hydraulic falls in two-layer flows. *J. Fluid Mech.* 234 (1992) 583–612.
13. S.R. Belward and L.K. Forbes, Fully non-linear two layer flow over arbitrary topography. *J. Eng. Math.* 27 (1993) 419–432.
14. M. Ikawa and Y. Nagasawa, A numerical study of a dynamically induced foehn observed in the Abashiri-Ohmu area. *J. Met. Soc. Japan* 67 (1989) 429–458.
15. R.B. Smith, On severe downslope winds. *J. Atmos. Sci.* 42 (1985) 2597–2603.
16. W.R. Peltier and J.F. Scinocca, The origin of severe downslope windstorm pulsations. *J. Atmos Sci.* 47 (1990) 2853–2870.
17. L.K. Forbes, Critical free-surface flow over a semi-circular obstruction. *J. Eng. Math.* 22 (1988) 3–13.
18. L.K. Forbes, Two-layer critical flow over a semi-circular obstruction. *J. Eng. Math.* 23 (1989) 325–342.
19. L.K. Forbes and L.W. Schwartz, Free-surface flow over a semicircular obstruction. *J. Fluid Mech.* 114 (1982) 299–314.
20. V.J. Monacella, *On Ignoring the Singularity in the Numerical Evaluation of Cauchy Principal Value integrals.* Hydromechanics Laboratory research and development report no. 2356, David Taylor Model Basin, Washington D.C., (1967).